JCTC Journal of Chemical Theory and Computation

Article

pubs.acs.org/JCTC

A Kinetic Monte Carlo Study of Fullerene Adsorption within a Pc-PBBA Covalent Organic Framework and Implications for Electron Transport

Brian T. Koo, Philip G. Berard,† and Paulette Clancy*

School of Chemical and Biomolecular Engineering, Cornell University, Ithaca, New York 14850, United States

Supporting Information

ABSTRACT: Two-dimensional covalent organic frameworks (COFs), with their predictable assembly into ordered porous crystalline materials, tunable composition, and high charge carrier mobility, offer the possibility of creating ordered bulk heterojunction solar cells given a suitable electron-transporting material to fill the pores. The photoconductive (hole-transporting) properties of many COFs have been reported, including the recent creation of a TT-COF/PCBM solar cell by Dogru et al. Although a prototype device has been fabricated, its poor solar efficiency suggests a potential issue with electron transport caused by the interior packing of the fullerenes. Such packing information is absent and cannot be obtained experimentally. In this paper, we use Kinetic Monte Carlo (KMC) simulations to understand the dominant pore-filling mechanisms and packing configurations of C_{60} molecules in a Pc-PBBA COF that are similar to the COF fabricated experimentally. The KMC simulations thus offer more realistic filling conditions than our previously used Monte Carlo (MC) techniques. We found persistently large separation distances between C_{60} molecules that are absent in the more tractable MC simulations and which are likely to hinder electron transport significantly. We attribute the looser fullerene packing to the existence of stable motifs with pairwise distances that are mismatched with the underlying adsorption lattice of the COF. We conclude that larger pore COFs may be necessary to optimize electron transport and hence produce higher efficiency devices.

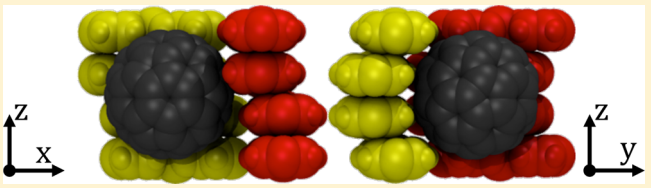

1. INTRODUCTION

Covalent organic frameworks (COFs) are a class of lightweight, porous, 2D and 3D materials,[1−4] which have become the subject of considerable activity for their potential as novel materials for gas storage,[5,6] catalysis,[7,8] selective separations,[9] and sensing.[10] More recently, crystalline 2D COFS have also begun to be explored experimentally[11−15] and computationally[16,17] for potential application in solar cells. COFs can be assembled from a number of organic fragments belonging to a set of "linkers" or "connectors,"[18] many of which are light-absorbing or charge-carrying moieties, including phthalocyanine,[19] porphyrin,[20] pyrene,[21] thiophene,[22] and thienothiophene.[11] The linkers and connectors assemble predictably to produce layered materials containing regular arrays of pores with square, hexagonal, or triangular cross-sectional areas. While the aromatic nature of the layers enables $\pi-\pi$ stacking, and thus hole transport perpendicular to the stacked sheets, the pore geometry guides the formation of a secondary phase of complementary electron-conducting molecules to enable electron transport.

The inherent design flexibility of covalent organic frameworks lets us construct ordered bulk heterojunction architectures[23] with the potential to reduce charge recombination, minimize charge trapping, and increase charge carrier mobility. Indeed, one such solar cell consisting of a two-dimensional thienothiophene-COF (TT-COF) filled with phenyl-C61-butyric acid methyl ester (PCBM) has already been made.[11] Although the power conversion efficiency of this TT-COF/PCBM was less than 1%, well below the roughly 10% efficiency needed for a viable photovoltaic device, the low efficiency of this prototype solar cell is partly due to the difficulty of filling two-dimensional COFs with fullerene molecules. Experimental techniques used to probe the contents of the pores, such as UV/vis spectroscopy, are insufficient to measure the distances between adsorbed fullerene molecules.[11] Experimentally, the packing density of the fullerene inside the COF was about 50% of that for bulk PCBM. In a recent publication,[16] we studied a similar COF, Pc-PBBA, with somewhat smaller (2.3 nm) square pores and determined that the 50% filling observed experimentally is actually very close to the theoretical maximum filling with C_{60} molecules predicted by traditional Monte Carlo techniques.

In this paper, we focus on understanding the filling process of the prototypical light-absorbing phthalocyanine phenylene-bis(boronic acid) covalent organic framework (Pc-PBBA)[19] with the prototypical fullerene molecule, C_{60}. Understanding the filling process is important because it establishes the final location of fullerene molecules inside the pores of the COF. This, in turn, affects the mechanistic pathways by which electrons percolate through the C_{60}-filled pores of the COF. A continuous percolation path for electrons is a prerequisite for

Received: November 22, 2014

DOI: 10.1021/ct501044u
J. Chem. Theory Comput. XXXX, XXX, XXX−XXX

an efficient solar cell; hence the existence of C_{60} "vacancies" would significantly decrease electron mobility and hence device performance. This need to understand the dynamics through which COF pores become filled is the motivation for the study described here.

The most appropriate choice of computational techniques to simulate the dynamics of pore-filling is less clear. As we reported earlier,[16] conventional computational methods such as Molecular Dynamics (MD) cannot simulate the diffusion or aggregation of fullerene molecules in COF pores because the time scales of these processes are far greater than what is accessible with MD. Monte Carlo (MC) simulations, which we have used[16] to describe possible final configurations of fullerene molecules in the pore, ignore the energetic landscape of adsorption sites in the pore and result in artificial configurations with much higher density.

Hence, in this paper we apply our previously generated catalog of energy barriers to a Kinetic Monte Carlo (KMC)[24] algorithm to simulate the filling mechanisms of fullerenes in COF pores. KMC allows us to explore time scales that are orders of magnitude longer than MD. It also allows us to observe the concerted diffusion of many fullerene molecules over microsecond or millisecond timeframes to fill an entire COF pore that is on the order of a hundred layers thick. However, since the electronic coupling between C_{60} molecules drops off exponentially with distance,[25] even a small perturbation of the location of the fullerene molecules can significantly change the mobility by orders of magnitude. Thus, we were concerned that the site-to-site hopping between KMC-defined lattice sites that is an intrinsic characteristic of KMC methods might not accurately define the fullerenes' locations. Hence, we used the results of the KMC simulations as the input to subsequent MD simulations to allow the fullerenes to relax to positions that are governed deterministically by the intermolecular forces in the system and not by the lattice sites inherent in the KMC simulation.

2. METHODS

2.1. Molecular-scale Topography of a Pc-PBBA COF Pore. The Pc-PBBA pores are square and 2 nm wide, and approximately double the 10 Å diameter of a C_{60} molecule. We, and others, have determined computationally that Pc-PBBA COF layers stack with a 1.4−1.7 Å translational offset[3,18] that is rotationally invariant. This stacking behavior produces porous channels with a rough interior topography that retards the transport of fullerene molecules, whose primary diffusion mechanism is along the surface. We discovered that the surface diffusion barriers increased from 2 to 10 kcal/mol when idealized, perfectly eclipsed pores were compared to more realistic helical and zigzag patterned pores. However, while the stacking of Pc-PBBA layers may be conveniently assigned to regular patterns like zigzag, helical, or staircase, our studies predicted that the stacking of layers is random.[18]

More recently, we modeled fullerene diffusion in COF pores by locating the metastable adsorption sites of fullerene molecules within solvent-filled pores and assigning energy barriers to transitions between them.[16] We improved our model in this paper by refining the interactions between fullerene and the interior of the pore as described in section 1 in the Supporting Information, and we include fullerene−fullerene interactions to more realistically model diffusion dynamics under high loading. The updated metastable adsorption sites are listed in Table 1 as lattice sites in our model. We carry out kinetic Monte Carlo simulations to determine the final packing configurations of fullerene molecules in many representative structures.

Table 1. Representative Stacking Patterns of Pc-PBBA Structures[a]

stacking pattern	sequence of layer offsets to produce stacking pattern
helical (H)	$[\leftarrow\uparrow\rightarrow\downarrow]_N$
staircase (SC)	$[\uparrow\uparrow\uparrow\uparrow]_N$
zigzag (ZZ)	$[\uparrow\downarrow\uparrow\downarrow]_N$
staircase-zigzag (SCZZ)	$[\uparrow\uparrow\downarrow\downarrow]_N$
helical-staircase (HSC)	$[\uparrow\rightarrow\uparrow\rightarrow]_N$

[a]Arrows in repeated sequences of layer offsets indicate direction (↑north, ↓south, →east, ←west) in the plane of the Pc-PBBA layers.

2.2. Monte Carlo. We used Metropolis Monte Carlo to find the theoretical maximum capacity of all corrugated structures studied in this paper. Taking the collection of adsorption sites as points in a lattice, we defined an insertion event that places a C_{60} molecule at any unoccupied lattice site, if at least 10 Å from every other C_{60} molecule. We also defined an artificial diffusion event that moves a C_{60} molecule to any lattice site within 10 Å of its initial position, if the destination site is similarly unoccupied and unblocked. We carried out 100 000 iterations of alternating insertion and diffusion events per simulation and repeated each simulation 20 times. We did not implement deletion events, but there were no outlying final C_{60} counts in any of the 20 simulations carried out for each corrugation pattern.

2.3. Kinetic Monte Carlo Algorithm. We used a Kinetic Monte Carlo algorithm[24] to simulate the filling process. Our KMC algorithm simulates two types of events: the addition of a new fullerene molecule onto an unoccupied site at the entrance of the pore at a rate of 1 fullerene/ns and diffusion of a randomly selected fullerene molecule to a nearby unoccupied lattice site. Each event is chosen according to its propensity and carried out. After each event is completed, the list of possible events and their propensities are updated. The KMC algorithm simulates the passage of time from a random sampling of time scales derived from the inverse of the sum of the propensities of all events. We carried out up to 10 billion iterations in each KMC simulation.

2.4. KMC Diffusion Barriers. Our kinetic Monte Carlo simulation of the Pc-PBBA pore includes 2432 unique vertical diffusion events (up and down the pore) and 832 unique lateral diffusion events (around the circumference of the pore). The distinction between vertical and lateral diffusion events can be found in section 1 of the Supporting Information. The complete catalogue of diffusion barriers is distinguished by direction (vertical or lateral) and plotted in Figure 1. The midpoint of each bar is the activation energy for that particular diffusion event, and the height equals twice the standard error of each event. The vertical diffusion barrier heights form a normal distribution with an average of 6.2 kcal/mol and standard deviation of 2.3 kcal/mol. The lateral diffusion barrier heights also form a normal distribution with an average of 10.5 kcal/mol with a standard deviation of 2.7 kcal/mol. The vertical diffusion barriers peak at 14.1 kcal/mol with a low of 0.0 kcal/mol, while the lateral diffusion barriers peak at 19.2 kcal/mol with a low of 3.8 kcal/mol.

The coordinates of each vertical and lateral diffusion pathway were averaged from an ensemble of pathways gathered from

DOI: 10.1021/ct501044u
J. Chem. Theory Comput. XXXX, XXX, XXX−XXX

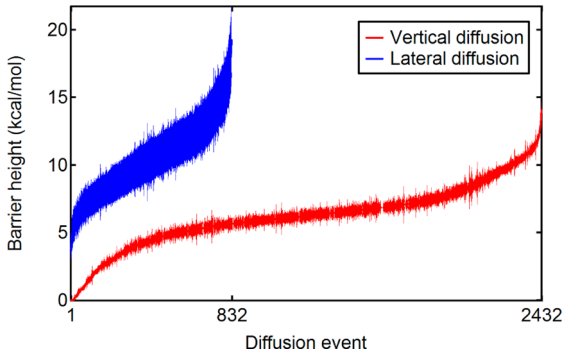

Figure 1. Vertical and lateral diffusion barriers with estimated error bars averaging approximately 0.3 kcal/mol for vertical barriers and 1.5 kcal/mol for lateral barriers.

Steered Molecular Dynamics (SMD) simulations[26] between established beginning and ending sites. The vertical diffusion events have relatively lower standard errors than lateral diffusion events because each pathway follows a well-defined minimum energy pathway running along the corner of the pore. In contrast, lateral diffusion events traverse higher energy potential energy surfaces with more options for diffusion.

The variability of the Pc-PBBA layers produces barrier heights that span many orders of magnitude. For instance, among the vertical diffusion events shown in Table S1, vertical pathways 69 and 136 both have 0.0 kcal/mol barrier heights. Vertical pathway 69 connects the **SCH1** and **H1SC** lattice sites, and the unique pairing of **SCH1** and **H1SC** produces a diffusion pathway with no barrier to diffusion due to the exact alignment of the low-barrier exits of the two anisotropic potential energy basins located at each lattice site. The unique arrangement of Pc-PBBA layers in pathway 136 minimizes the barrier height by reducing the distance between the **SC** and **ZZ** lattice sites to less than the interlayer spacing of Pc-PBBA (3.34 Å). The largest vertical diffusion barrier is present in vertical pathway 50, where fullerenes diffuse between two zigzag lattice sites. Of the lateral diffusion pathways in Table S2, pathways 32 and 21 have the lowest and highest barriers, respectively.

2.5. Assumptions. We made a number of assumptions to reduce the combinatorial complexity of the KMC simulations. To describe diffusion of fullerene within the pore, we consider only the more frequent surface diffusion and not the rarer surface desorption and adsorption events. Since the 2.0 nm width of the Pc-PBBA pore is the equivalent of two fullerene molecules arranged side by side, desorption mechanisms are unlikely to impact the dynamics of transport within the pore. We impose a rapid insertion rate of 1 C_{60}/ns to arrive quickly at the more relevant final packing configurations, rather than the less relevant diffusion mechanisms. A more reasonable estimate based on the flux of fullerene in a saturated chlorobenzene solution into an empty Pc-PBBA COF pore should be on the order of one C_{60}/s. Under the assumption of one C_{60}/ns, the adsorption rate of fullerene begins artificially high but slows by orders of magnitude under higher loading.

Within the Arrhenius law used to calculate rates of diffusion from a prefactor and activation barrier, we assigned the same prefactor to all rates of diffusion. We estimated a prefactor by measuring the frequency of diffusion of a single fullerene in a solvent-filled, staircase-stacked COF pore with known diffusion barrier heights. Our calculation estimates the prefactor to be 5×10^{11} s^{-1}. We chose the staircase-stacked COF pore to obtain an estimate for the prefactor because the surface diffusion barriers are the smallest and most uniform on this pore surface.

3. RESULTS AND DISCUSSION

3.1. Visualization of our KMC Framework of Diffusion Pathways. The KMC framework for the five representative structures (helical, helical-staircase, staircase-zigzag, staircase, and zigzag) at zero loading is shown in Figure 2 as a visualization of all diffusion pathways, colored by the energy of the potential of mean force of each pathway. The lattice sites are discernible in the framework by their low energy (shown in blue in Figure 2), while the many overlapping diffusion pathways between them are shown to conform to the surface of the pore. The vertical diffusion pathways are the most direct between adjacent lattice sites, while the lateral diffusion pathways are more circuitous and higher in energy. The less direct a pathway, the more likely it is to become unfavorably blocked by the occupancy of a neighboring lattice site. Therefore, lateral traversal in the helical, helical-staircase, and staircase-zigzag structures are comparatively rarer than lateral traversal in the staircase or zigzag structures. Because lateral diffusion pathways aid in the reorganization of fullerene in the

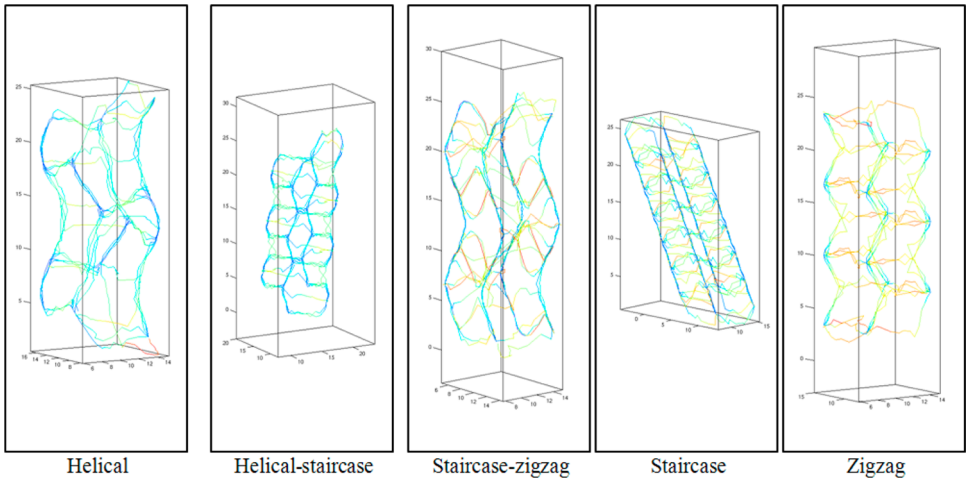

Figure 2. Diffusion pathways in representative structures. The colors refer to the height of the energy barrier, ranging from a low barrier (blue) of −5 kcal/mol to a high barrier (red) of 20 kcal/mol with intermediate barriers shown in yellow.

DOI: 10.1021/ct501044u
J. Chem. Theory Comput. XXXX, XXX, XXX−XXX

pore, the helical, helical-staircase, and staircase-zigzag structures can be expected to contain more vacancies.

Under the rules we imposed within the KMC framework, it is evident that the filling process is impeded by a number of constraints. The locations of lattice sites, which were determined under the conditions of an empty pore, are heavily coarse-grained and allow diffusion to be tractably described within the pore. However, this limits fullerene diffusion on a lattice. Under this approximation, we assume that fullerene molecules interact strongly with the Pc-PBBA inner surface at discrete sites and cannot form close-packed structures with other fullerene molecules if the occupied lattice sites are not about 10 Å apart. With lattice sites such as **SC** that do not bind strongly with fullerene molecules, fullerene may prefer off-lattice positions in the vicinity of other fullerene molecules to form more stable close-packed clusters. We also observe that fullerene mobility is sensitive to the sequence of the interlayer offsets that give rise to the Pc-PBBA structure. As a case in point, lateral offset sequences found in the helical, staircase-zigzag, and zigzag structures effectively reduce the pore size and prevent fullerene molecules from diffusing past other fullerene molecules in the pore. Thus, on the way to maximum capacity, the filling process is rate-limited by the probability of lateral traversal, which—in some pathways—goes to zero.

3.2. Distribution of Fullerene in Final Packing Configurations. *3.2.1. Distance between Fullerene Molecules in Filled Pores.* The final arrangement of fullerene sensitively depends on the structure of the Pc-PBBA pore. Our choice of representative structures, listed in Table 1, spans repeated local patterns of either two layers (staircase, zigzag, helical-staircase) or four layers (helical, staircase-zigzag), as well as a set of randomly generated structures. These structures are intended to sample the entire range of lattice sites and surface diffusion barriers that might be expected to affect packing and filling within the pore. The density of lattice sites determines the tolerance of a structure to accommodate close-packed configurations of fullerene molecules, which—in turn—is important for electron transport, enabled through electron-hopping between fullerenes. The diffusion barriers connecting adjacent lattice sites determine the kinetics of filling and the degree to which fullerene molecules remain either "on" or "off" our set of lattice sites.

The arrangement of fullerene molecules that fill the pore as a result of the kinetic Monte Carlo simulation is, not surprisingly, less dense than the analogous Monte Carlo (MC)-simulated result, as shown in Figure 3. The filling process simulated by KMC requires each fullerene in the final configuration to have followed a diffusive pathway beginning at the entrance of the pore. Combining this restriction with the coarseness of the diffusion pathways connecting the lattice sites means that fullerene molecules may not have the ability to rearrange into denser patterns. The net result is that the pores fill to less than maximum capacity. In contrast, MC allows the filling process to insert a fullerene wherever there is a vacancy, without regard to how it got there. Although such trial moves are clearly nonphysical, MC is a useful way to quickly determine the maximum possible number of fullerene molecules that can be accommodated inside the COF pore (ideal filling). The comparison of the resulting structures from MC and KMC is thus a useful way for us to locate kinetically trapped configurations and defects.

The overall distribution of distances between fullerene molecules in the pore, which influences charge transport, can

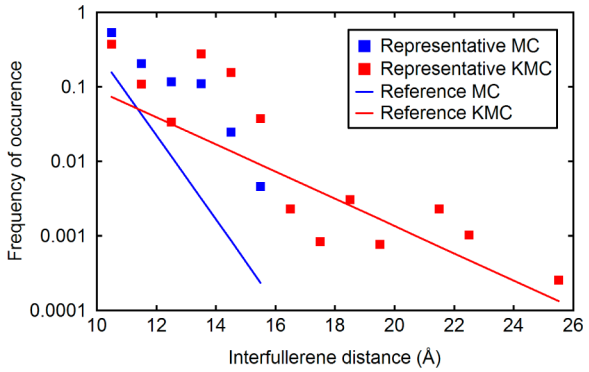

Figure 3. Representative MC and KMC data show the frequency of finding certain interfullerene distances in filled pores. The solid lines represent exponential curves fitted to interfullerene distances in 500 filled, randomly patterned 15-layer pores as found in MC (blue) and KMC (red) simulations. Again, distances are computed from the shortest cumulative path connecting fullerene molecules in the pore.

be fitted as an exponential function (Figure 3). We simulated pore-filling with complementary KMC and MC methods as a means to obtain information on kinetically accessible configurations of fullerene as well as establish their theoretical maximum filling capacities. Our analysis, which includes only the distances between fullerene molecules that are necessary to form the shortest connecting path through the pore, ignores any analysis of fullerene molecules that branch off the shortest chain. This is a reasonable assumption since such moves offer much slower pathways for charge transport.

The distribution of distances shown in Figure 3 identified frequently occurring patterns of low-count tightly packed fullerene motifs (clusters). Our results have shown that these small packing motifs are important; the close distances between fullerene molecules that occur in each of these motifs suggest that cluster formation is a stable process and that the filling process is rate-limited by the diffusion and dissociation of these clusters.

3.2.2. Interfullerene Distances and Frequencies. The distribution of distances between fullerene molecules belonging to the shortest chain inside the pore for randomly stacked layers follows eq 1 for the MC simulation and eq 2 for the KMC simulation.

$$F^{\mathrm{MC}} = 0.8\mathrm{e}^{-1.1(d-10.0)} \quad (1)$$

$$F^{\mathrm{KMC}} = 0.1\mathrm{e}^{-0.4(d-10.0)} \quad (2)$$

In these equations, F is the frequency of occurrence and d is the distance between fullerenes. The equations were fitted to a sample of 500 randomly patterned pores of 15 layers for MC and 15 layers for KMC. The arrangement of fullerenes in the pore has no long-range order. Thus, by compiling interfullerene distances in a collection of small pores, we can reconstruct the true distribution of interfullerene distances in a larger pore, assuming infinite filling time. Our KMC simulations were somewhat limited in their ability to simulate the complete filling of the pores due to the variation of diffusion barriers requiring long time scales. The small size of the 15-layer pores may erroneously introduce larger distances between fullerenes toward the ends of the pore. This would skew the distribution toward larger distances. To compensate for this artifact, we have truncated our data past 20 Å.

DOI: 10.1021/ct501044u
J. Chem. Theory Comput. XXXX, XXX, XXX−XXX

The MC-derived and KMC-derived distributions show very dissimilar trends. The KMC distribution starts lower in frequency and decays more slowly than the MC distribution. In the KMC simulations, we find that kinetically accessible configurations exhibit relatively fewer close-packed fullerenes in the 10−11 Å range and relatively larger average distances between fullerenes. Although the KMC simulation produces motifs of closer-packed fullerenes, the nature of MC simulations favors final configurations that include more distances in this range. With a higher resolution, we observe that MC simulations populate the 10−11 Å range uniformly, while the KMC simulations favor distances closer to 10 Å. Overall, the KMC distribution predicts a lower final count of fullerene molecules. The number of these vacancy defects, which include distances greater than 20 Å, can be predicted according to the distribution given in eq 2. This can then be scaled with the number of layers in the pore to predict the statistical frequency and severity of these defects.

On the other hand, the MC distribution shows that a pore achieving maximum capacity adopts a much narrower interfullerene distance distribution. The frequency of defects drops off much more steeply with no configuration having an interfullerene distance larger than 16 Å (roughly 1.6 times the diameter of a single fullerene). This result is expected because KMC inevitably exhibits kinetically inaccessible pathways (which lead to larger or more frequent vacancies), whereas the MC method allows it to fill pores without such restrictions. Interestingly, the overall KMC frequency distribution attained from summing the individual frequencies of our five simple patterned pores conformed to the random distribution attained from analyzing 500 randomly generated pore structures. This observation did not hold for the MC simulations of our five simple patterned pores, as the combined frequency distribution was skewed toward larger distances. MC simulations of randomly generated pores ignore the relative stability of each lattice site and are prone to fill pores without favoring close-packed motifs of fullerene. Given that the distributions of fullerene distances within our five chosen representative structures (Table 1) matched the broader distribution of fullerene distances in 500 randomly generated structures, we can generalize our analysis of specific motifs to the broader class of random structures.

3.2.3. Characteristic Fullerene Cluster Motifs. We postulated that the distribution of fullerene in each representative structure in Table 1 could be explained in terms of the smallest packing unit (motif). Therefore, we identified unique clusters of fullerenes as a motif and assigned characteristic distances to each one. Of all pairwise distances between fullerene molecules in the pore, we only considered distances that were part of the shortest connected pathway (linking center of masses of fullerene molecules) through the pore. This method only samples pairwise distances important to electron percolation through the pore. We round distances between fullerenes to the nearest quarter angstrom and state distances according to the lower bound of each range (*i.e.*, "10 Å" would signify distances between 10.00 and 10.25 Å). The choice of a resolution of 0.25 Å was the largest value that could still differentiate motifs in different structures. In the following subsections, we identify unique motifs present in significant quantities in each representative structure and describe differences between the packing configurations found with kinetic Monte Carlo and Monte Carlo.

3.2.3.1. Helical. In the helical patterned pore, we observe a difference in the most prevalent motifs found in KMC and MC simulations. The KMC simulation found clusters consisting of mostly 3-fullerene motifs, with characteristic distances of 10.25 and 10.75 Å (Figure S1). On the other hand, the MC simulation found an abundance of 4-fullerene motifs with characteristic distances of 10.75 and 11.00 Å (Figure S1). Interestingly, the 3-fullerene motifs found in KMC simulations do not appear in *any* MC simulated configurations because this motif, although more compact, does not tessellate on the helical lattice. The 4-fullerene motif, although less stable than the 3-fullerene motif, is more compatible with the helical lattice and maintains a higher uniform density. As shown in Figure 4, the

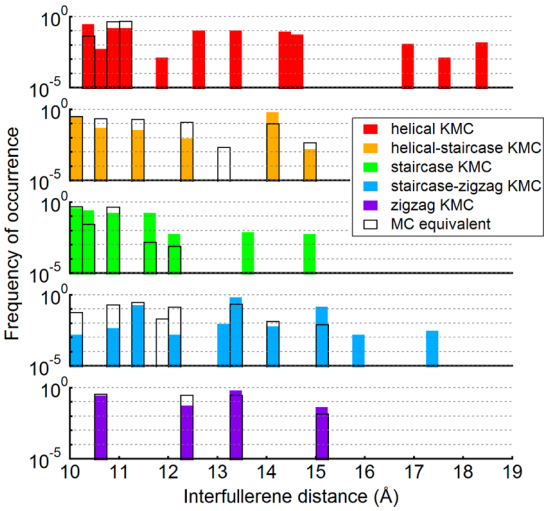

Figure 4. Compilation of interfullerene distances in the pore, sampled from final snapshots of KMC (solid) and MC (hollow) simulations of filling helical, helical-staircase, staircase, staircase-zigzag, and zigzag patterned pores with fullerenes. Distances are computed from the shortest cumulative path connecting fullerene molecules in the pore. Data for each pattern were compiled from 20 simulations each.

frequency plot indicates most motifs in the KMC simulation are of the 3- and 4-fullerene variety, while most motifs in the MC simulation are composed of 4-fullerenes. In the KMC simulation, there is also a significant frequency of occurrence at 12.50 Å, 13.25 Å, and 14.25 Å due to the distances between 3-fullerene motifs and between 3- and 4-fullerene motifs.

3.2.3.2. Staircase. In the staircase-patterned pore, the distribution of fullerenes is best described as pairs of fullerenes 10.00 Å apart contacting other pairs of fullerenes in the pore in three distinct orientations, with characteristic distances of 10.25 Å, 10.75 Å, and 11.50 Å, as shown in Figure S3. Only one contact orientation, with a characteristic distance of 10.75 Å, tessellates the staircase lattice and produces the highest density filling. The MC simulation produces packing configurations that correspond primarily to this contact orientation. The KMC simulation favors the 10.25 Å contact orientation, but only slightly more than the other two because this contact motif does not tessellate the staircase lattice. Because this motif contains the more energetically favorable distance of 10.25 Å, the KMC simulation produces more of these motifs and, as a result, fills at a lower density.

3.2.3.3. Zigzag. The primary motif in the zigzag-patterned pore in both MC and KMC simulations is a pair of fullerenes 10.50 Å apart occupying opposite corners of the pore. There

DOI: 10.1021/ct501044u
J. Chem. Theory Comput. XXXX, XXX, XXX−XXX

are two possible contact orientations between pairs of fullerenes, giving rise to characteristic distances of 12.25 Å and 13.25 Å. The KMC simulations produce configurations with mostly 13.25 Å contacts, while the MC simulations yield configurations with equally weighted 12.25 Å and 13.25 Å contact configurations. Both contact types fill the zigzag pore with the same number of fullerenes. The distance of 12.25 Å arises from an antiparallel alignment of pairs that is not frequently observed in KMC simulations because this distance falls between the zero-solvent shell and first solvent shell between fully solvated fullerenes, located at separations of 10.00 Å and 13.50 Å, respectively.

3.2.3.4. Staircase-zigzag. There are no motifs within the staircase-zigzag patterned pore because the energetic landscape of the lattice is punctuated by strong adsorption sites separated by relatively large distances of 11.25 Å, 13.25 Å, and 15.00 Å. The loose filling of fullerenes in this pore can be explained by the partitioning of the pore into two identical channels, where the diffusion pathways between channels are 10 orders of magnitude slower than diffusion pathways within channels. The KMC simulation, as shown in the final snapshot of Figure S6, shows fullerenes filling nonuniformly on the left and right sides of the pore. Each fullerene randomly selects the left or right channel and diffuses into the right channel due to a biasing of diffusion pathways between the top lattice sites of the pore, where the fullerenes remain for most of the simulation. Fullerenes within the channel have characteristic separation distances of 13.25 Å and 15.00 Å. For fullerenes across channels, the characteristic distances are 11.25 Å and 13.25 Å. On the other hand, the MC simulation produces varied distances because it ignores the relative stability of lattice sites and therefore ignores the phenomenon of two-channel diffusion.

3.2.3.5. Helical-staircase. The helical-staircase patterned pore is primarily filled by pairs of fullerene 10.00 Å apart, with only one possible contact orientation between pairs giving rise to a distance of 14.00 Å. The energetic landscape of the helical-staircase pore can be partitioned into two dissimilar channels, where diffusion of fullerene within the primary channel is orders of magnitude faster than diffusion within the secondary channel. The diffusion across channels is similarly slow. We observe that the primary channel transports isolated fullerene molecules to other fullerenes in the pore, where—on contact—they migrate to the secondary channel, where the observed pair motif resides. Since the MC simulation ignores the energetic landscape and performs an unbiased filling, the distances in the final configurations are varied and incomparable to those of the KMC simulations.

3.3. Filling Curves in Representatively Patterned Pores. As shown in Figure 5, of the representative patterns we studied, the staircase and zigzag filling curves form lower and upper bounds, respectively, to the speed of the filling process. However, because the staircase structure contains the smallest diffusion barriers on average and the zigzag structure contains the largest ones, the filling curves of randomly generated structures should also be bounded by the staircase and zigzag curves. The exact shape of the random curve will be dependent on the proportion of the six lattice site types listed in Table 2 that characterize a particular random structure. The existence of a greater proportion of SC lattice sites will hasten filling. A greater proportion of zigzag lattice sites will slow filling. The speed of filling other lattice site types will fall in-between these limits. KMC simulations of helical-staircase and

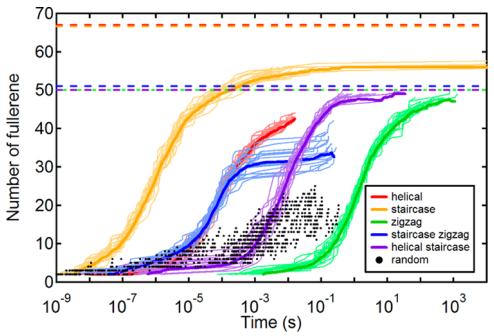

Figure 5. Filling over time in pores with the following stacking patterns: helical (red), staircase (yellow), zigzag (green), staircase-zigzag (blue), helical-staircase (purple), and randomly patterned pores (black filled circles). The dashed lines show the theoretical maximum capacities found by Monte Carlo simulations.

Table 2. Catalogue of Lattice Site Types

lattice type	example offset sequence and corner location to produce lattice type (NE = northeast corner)
H1	→↓ (NE)
H2	↑→ (NE)
ZZ	↑↓ (NE)
SC	↑↑ (NE)
H1H2 or H2H1	↑→↓ (NE)
SCH1 or H1SC	→→↓ (NE)

zigzag pores achieve the theoretical maximum capacity, while the helical, staircase, and staircase-zigzag patterns saturate below capacity due to the existence of motifs that stabilize nontessellating configurations of fullerenes. We define the capacities of each pore from 500 MC simulations of each structure.

For the zigzag and helical-staircase structures (Table 1), the loading of the pore enhances the diffusion of fullerenes to produce more uniformly filled pores, while the helical and staircase-zigzag pore patterns are adversely affected. For each representative structure, we identified specific sequences of diffusion events occurring on separate time scales that explained the variation in the distribution of distances between fullerene in KMC-filled pores and MC-filled pores. In a majority of identified sequences, we found frequent occurrences of intermediate configurations of fullerenes that were 10.0 Å and 13.7 Å apart, given that these distances stabilize the fullerene−fullerene interaction with zero solvent and one solvent shell, respectively. Our representative pores repeat simple sequences of layer offsets, so diffusion mechanisms within randomly patterned layers are less comparable. However, by analyzing each pattern, we can describe how the kinetics of filling affect the final arrangements of fullerenes in some pores and explain the intractable nature of filling in other pores. We describe some of the major diffusion mechanisms in a representative Pc-PBBA pore pattern in section 2 of the Supporting Information.

3.3.1. Randomly Offset Pore Structures. We generated three randomly patterned pores to measure the effect of stacking variability on filling kinetics and found incomplete filling in all trials. Our KMC simulation filled far below pore capacity given that (a) increased kinetic trapping prevents fullerene molecules from reorganizing into denser configurations and (b) the theoretical maximally filled configurations

DOI: 10.1021/ct501044u
J. Chem. Theory Comput. XXXX, XXX, XXX−XXX

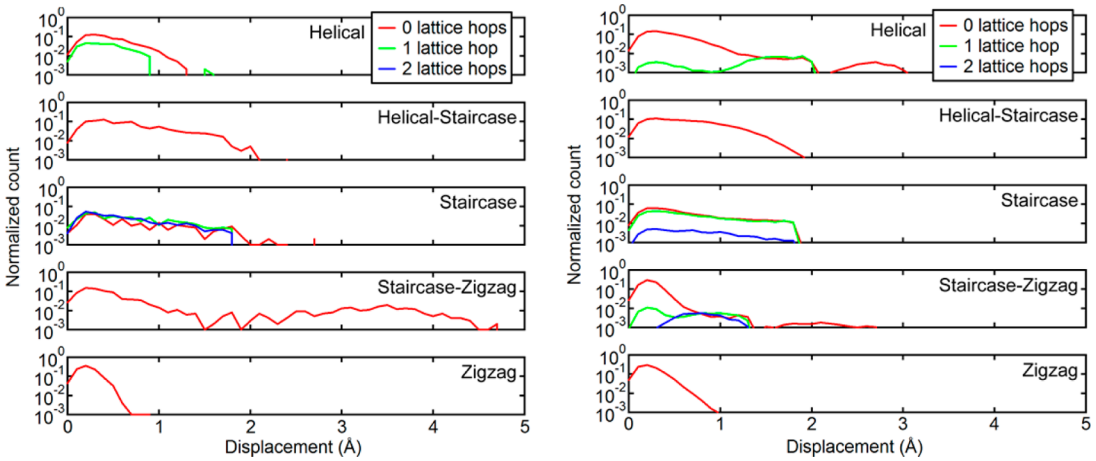

Figure 6. Molecular dynamics trajectories of fullerene at zero pore-loading (left) and full pore-loading (right) in representative structures.

are computationally inaccessible. However, during the early stages of the filling process, the curves all lie between the quick progression of the staircase and the limiting progression of the zigzag filling curves. Since our 100-layer randomly generated structures contain some proportion of zigzag lattice sites, we expected the random curves to fill slower than the other four representative patterns. Once the random curves reach time scales relevant for zigzag growth between 10^{-2} and 10^{0} seconds, we anticipate the random curves will enter the steepest phase of growth, mirroring the paths that the other representative filling curves have followed.

3.4. Molecular Dynamics Simulations of Off-lattice Defects. We studied the prevalence of off-lattice behavior of fullerenes by conducting Molecular Dynamics (MD) simulations using snapshots of the pore provided by our KMC simulations as the starting point. Our fully atomistic MD simulations relax the assumption of discrete lattice positions and include individual chlorobenzene molecules to solvate the interior of the pore and surrounding volume. We analyzed singly loaded pores of each representative structure to establish a reference for our analysis of filled pores. For each structure in Table 1, we created a histogram of the displacement of each fullerene from its nearest lattice site in the KMC framework, shown in Figure 6. Fullerenes that are closer to some other lattice site along its trajectory are assigned to a separate histogram. Our MD simulations were 1 ns long and performed under the constant-volume, constant-temperature NVT ensemble with the Nosé−Hoover thermostat[27] at 300 K with a temperature damping parameter of 100 fs and a time step of 1 fs. We model the rigid COF layers with the Dreiding force field,[28,29] the fullerene molecules with OPLS,[30] and explicit chlorobenzene solvent molecules with OPLS. Details of our methodology for solvating loaded Pc-PBBA pores with chlorobenzene solvent can be found in section 9 of the Supporting Information.

As shown in the histograms of singly loaded pores, our KMC lattice reproduces the effect of a full MD simulation, since most displacement histograms are sharply peaked at one value. The staircase-zigzag structure shows off-lattice behavior, but this is an artifact of the fullerene exiting the pore. In the helical-staircase and zigzag structures, the plots show a stationary fullerene located at its originally assigned lattice site. In the helical and staircase patterned pores, the fullerene diffuse to one and two neighboring lattice sites, respectively. The peak heights of the secondary and tertiary displacement histograms explain the relative stability of neighboring lattice sites. The peak heights of the primary and secondary displacement histograms in the helical structure differ by a factor of 3, which signifies the large surface barriers preventing diffusion. On the other hand, the peak heights of the primary, secondary, and tertiary displacement histograms in the staircase structure are all very similar, which suggests that fullerene diffuses rapidly between the three neighboring lattice sites even in a fully solvated pore.

We observe from our displacement histograms of filled pores that the distributions are similar to those of the unfilled pores. The plots show that off-lattice clustering is heavily prevalent in the staircase structure, mildly prevalent in the helical and staircase-zigzag structures, and nonexistent in the helical-staircase and zigzag structures. The displacement histograms in the staircase structure form a shoulder, which suggests the formation of many off-lattice fullerenes that are stabilized by neighboring fullerene. This highlights one disadvantage of our KMC framework, which is less accurate in situations where interactions between guest molecules are more significant than interactions between the guest molecule and COF surface. The helical and staircase pores produce histograms where approximately one-tenth of fullerenes are off-lattice.

In summary, higher diffusion barriers between lattice sites produce more relevant KMC simulations. Our representative staircase structure, with its low surface barriers, is inaccurately simulated by KMC, but structures like zigzag and staircase-zigzag are able to simulate the packing of fullerenes accurately. Because realistic structures are randomly stacked, this shortcoming is unlikely to affect filling and packing in any significant way.

3.5. Implications for Electron Transport. The electron mobility in bulk C_{60} is related to the electron hopping rate between C_{60} molecules, which can be modeled by semiclassical Marcus theory.[25] According to Marcus theory, the electron hopping rate between C_{60} molecules is proportional to the square of the electronic coupling, which exponentially decays by a factor of 10 per angstrom of separation. Thus, we directly compare distribution functions between physical vapor-deposited disordered C_{60} thin films and C_{60} adsorbed in Pc-PBBA pores to make a qualitative comparison of the electron mobility in both materials. The electron mobility of disordered C_{60} thin films studied by Kwiatkowski et al. was shown to be half the electron mobility in single crystal C_{60}.[25]

Our kinetic Monte Carlo simulations predict a distribution of C_{60}−C_{60} distances that peaks at 10 Å and decreases 10-fold for

DOI: 10.1021/ct501044u
J. Chem. Theory Comput. XXXX, XXX, XXX−XXX

every additional 6 Å of separation. In comparison, the computational study of disordered C_{60} thin films predicts a much tighter distribution of distances that also peaks at 10 Å but decreases much more quickly, 10-fold per 0.5 Å of separation.[25] The electron mobility of fullerene within the pore is, thus, likely to be far worse than that of disordered thin films, given the stark contrast between both distributions. Therefore, devices created from COF/fullerene materials may need either functionalized porous surfaces[31] to promote closer packed fullerene molecules, or increased pore size to increase the proportion of C_{60}-C_{60} to C_{60}-surface interactions.[32]

4. CONCLUSIONS

Our kinetic Monte Carlo simulations demonstrate the persistence of large gaps between C_{60} molecules in Pc-PBBA pores that cannot be predicted from conventional methods such as Monte Carlo or molecular dynamics. Our method captures both the rare frequency of diffusion and the kinetic trapping that occurs in pores. We found that the distribution of interfullerene distances decays exponentially by a factor of 10 every 6 Å, compared to more close-packed physical vapor-deposited C_{60}, which decays much faster, by a factor of 10 every 0.5 Å. The root cause of this short-range disorder is the intrinsic mismatch between the characteristic distances of stable fullerene motifs and the underlying surface lattice sites in the Pc-PBBA pores.

Mechanistically, the filling process in Pc-PBBA has proven to be very sensitive to the corrugation patterns of the pore. More realistic, randomly patterned structures will result in increased trapping, leading to lower loading capacities relative to an idealized eclipsed stacking pattern. Representative corrugation patterns have shown kinetic trapping to largely affect filling in helical and staircase-zigzag structures, whereas minimal trapping is observed in zigzag and helical-staircase structures, as demonstrated by comparison to Monte Carlo simulated filling. This result has profound negative implications for electron transport. Consequently, the design of higher performing COF/fullerene solar cells should employ COFs with larger pores or functionalized pores to minimize the effect of surface interactions. This would facilitate the creation of close-packed fullerene configurations that provide a facile percolating path for electrons that will give rise to higher electron mobilities.

■ ASSOCIATED CONTENT

Ⓢ Supporting Information

Additional information on the KMC algorithm used in this paper, edge defects and concerted diffusion mechanisms, snapshots of filled representative pores in KMC and MC, lists of vertical and lateral diffusion pathways, and solvation of loaded pores for atomistic MD simulations. This material is available free of charge via the Internet at http://pubs.acs.org/.

■ AUTHOR INFORMATION

Corresponding Author

*E-mail: pc@icse.cornell.edu.

Present Address

†MathWorks, Natick, MA 01760-2098, United States.

Notes

The authors declare no competing financial interest.

■ ACKNOWLEDGMENTS

The authors would like to thank the National Science Foundation through the "Nanoelectronics Beyond 2020" (NEB) program, award number CHE-1124754, and a gift from the NRI, award number (Gift # 2011-NE-2205GB) for financial support of this work. P.G.B. thanks Intel Corporation for its support via the College of Engineering's Engineering Learning Initiatives. P.G.B. also thanks the Xerox Foundation for their support of the F. Rodriguez Outstanding Student Award in Polymers and Electronic Materials, which P.G.B. was awarded in 2013 for this work.

■ REFERENCES

(1) Côté, A. P.; Benin, A. I.; Ockwig, N. W.; O'Keeffe, M.; Matzger, A. J.; Yaghi, O. M. *Science* **2005**, *310*, 1166−1170.
(2) Feng, X.; Ding, X.; Jiang, D. *Chem. Soc. Rev.* **2012**, *41*, 6010−6022.
(3) Ding, S.-Y.; Wang, W. *Chem. Soc. Rev.* **2013**, *42*, 548−568.
(4) Xiang, Z.; Cao, D. *J. Mater. Chem. A* **2012**, *1*, 2691−2718.
(5) Furukawa, H.; Yaghi, O. M. *J. Am. Chem. Soc.* **2009**, *131*, 8875−8883.
(6) Doonan, C. J.; Tranchemontagne, D. J.; Glover, T. G.; Hunt, J. R.; Yaghi, O. M. *Nat. Chem.* **2010**, *2*, 235−238.
(7) Ding, S.-Y.; Gao, J.; Wang, Q.; Zhang, Y.; Song, W.-G.; Su, C.-Y.; Wang, W. *J. Am. Chem. Soc.* **2011**, *133*, 19816−19822.
(8) Fang, Q.; Gu, S.; Zheng, J.; Zhuang, Z.; Qiu, S.; Yan, Y. *Angew. Chem., Int. Ed.* **2014**, *53*, 2878−2882.
(9) Tilford, R. W.; Mugavero, S. J., III; Pellechia, P. J.; Lavigne, J. J. *Adv. Mater.* **2008**, *20*, 2741−2746.
(10) Dalapati, S.; Jin, S.; Gao, J.; Xu, Y.; Nagai, A.; Jiang, D. *J. Am. Chem. Soc.* **2013**, *135*, 17310−17313.
(11) Dogru, M.; Handloser, M.; Auras, F.; Kunz, T.; Medina, D.; Hartschuh, A.; Knochel, P.; Bein, T. *Angew. Chem.* **2013**, *125*, 2992−2996.
(12) Feng, X.; Chen, L.; Honsho, Y.; Saengsawang, O.; Liu, L.; Wang, L.; Saeki, A.; Irle, S.; Seki, S.; Dong, Y.; Jiang, D. *Adv. Mater.* **2012**, *24*, 3026−3031.
(13) Wan, S.; Guo, J.; Kim, J.; Ihee, H.; Jiang, D. *Angew. Chem., Int. Ed.* **2008**, *47*, 8826−8830.
(14) Ding, X.; Chen, L.; Honsho, Y.; Feng, X.; Saengsawang, O.; Guo, J.; Saeki, A.; Seki, S.; Irle, S.; Nagase, S.; Parasuk, V.; Jiang, D. *J. Am. Chem. Soc.* **2011**, *133*, 14510−14513.
(15) Ding, X.; Guo, J.; Feng, X.; Honsho, Y.; Guo, J.; Seki, S.; Maitarad, P.; Saeki, A.; Nagase, S.; Jiang, D. *Angew. Chem., Int. Ed.* **2011**, *50*, 1289−1293.
(16) Koo, B. T.; Clancy, P. *Mol. Simul.* **2013**, *40*, 58−70.
(17) Patwardhan, S.; Kocherzhenko, A. A.; Grozema, F. C.; Siebbeles, L. D. A. *J. Phys. Chem. C* **2011**, *115*, 11768−11772.
(18) Koo, B. T.; Dichtel, W. R.; Clancy, P. *J. Mater. Chem.* **2012**, *22*, 17460−17469.
(19) Spitler, E. L.; Dichtel, W. R. *Nat. Chem.* **2010**, *2*, 672−677.
(20) Wan, S.; Gándara, F.; Asano, A.; Furukawa, H.; Saeki, A.; Dey, S. K.; Liao, L.; Ambrogio, M. W.; Botros, Y. Y.; Duan, X.; Seki, S.; Stoddart, J. F.; Yaghi, O. M. *Chem. Mater.* **2011**, *23*, 4094−4097.
(21) Wan, S.; Guo, J.; Kim, J.; Ihee, H.; Jiang, D. *Angew. Chem.* **2009**, *121*, 5547−5550.
(22) Bertrand, G. H. V.; Michaelis, V. K.; Ong, T.-C.; Griffin, R. G.; Dincă, M. *Proc. Natl. Acad. Sci. U. S. A.* **2013**, *110*, 4923−4928.
(23) Mayer, A. C.; Scully, S. R.; Hardin, B. E.; Rowell, M. W.; McGehee, M. D. *Mater. Today* **2007**, *10*, 28−33.
(24) Gillespie, D. T. *J. Comput. Phys.* **1976**, *22*, 403−434.
(25) Kwiatkowski, J. J.; Frost, J. M.; Nelson, J. *Nano Lett.* **2009**, *9*, 1085−1090.
(26) Park, S.; Schulten, K. *J. Chem. Phys.* **2004**, *120*, 5946−5961.
(27) Tuckerman, M. E.; Alejandre, J.; Lopez-Rendon, R.; Jochim, A. L.; Martyna, G. J. *J. Phys. A: Math. Gen.* **2006**, *39*, 5629−5651.

DOI: 10.1021/ct501044u
J. Chem. Theory Comput. XXXX, XXX, XXX−XXX

(28) Mayo, S. L.; Olafson, B. D.; Goddard, W. A., III. *J. Phys. Chem.* **1990**, *94*, 8897−8909.
(29) Song, X.-Z.; Jentzen, W.; Jia, S.-L.; Jaquinod, L.; Nurco, D. J.; Medforth, C. J.; Smith, K. M.; Shelnutt, J. A. *J. Am. Chem. Soc.* **1996**, *118*, 12975−12988.
(30) Jorgensen, W. L.; Maxwell, D. S.; Tirado-Rives, J. *J. Am. Chem. Soc.* **1996**, *118*, 11225−11236.
(31) Nagai, A.; Guo, Z.; Feng, X.; Jin, S.; Chen, X.; Ding, X.; Jiang, D. *Nat. Commun.* **2011**, *2*, 1−8.
(32) Spitler, E. L.; Colson, J. W.; Uribe-Romo, F. J.; Woll, A. R.; Giovino, M. R.; Saldivar, A.; Dichtel, W. R. *Angew. Chem., Int. Ed.* **2012**, *51*, 2623−2627.

DOI: 10.1021/ct501044u
J. Chem. Theory Comput. XXXX, XXX, XXX−XXX